Materials and Manufacturing Processes, 21: 87–96, 2006

ISSN: 1042-6914 print/1532-2475 online
DOI: 10.1081/AMP-200060636

Taylor & Francis
Taylor & Francis Group

Property Change During Fixtured Sintering of NiTi Memory Alloy

Sayed Khatiboleslam Sadrnezhaad[1] and Omid Lashkari[2]

[1]*Department of Materials Science and Engineering, Center of Excellence for Advanced Materials Production Processes, Sharif University of Technology, Tehran, Iran*
[2]*Department of Applied Sciences, University of Quebec at Chicoutimi, Chicoutimi, Quebec, Canada*

Fixtured sintering of up to 5 hours at 1223 to 1323 K is successfully used to diminish the dimensional change of NiTi memory alloys produced from mixtures of elemental Ni and Ti powders packed and pressed at room temperature under 400, 500, and 600 MPa pressure. The improvements obtained can help near-net-shape technology via powder metallurgy that overcomes the traditional casting problems such as oxygen, nitrogen, hydrogen, and carbon absorption and intermetallic compound precipitation, which lower the workability and the homogeneity of the final alloy. The effects of compaction pressure, sintering time, and sintering temperature on dimensional change, porosity, hardness, and morphology of the produced TiNi intermetallic alloy are investigated. Phase transformation temperatures and mechanical properties of the sintered samples were determined and compared for the influence of compaction pressure and sintering conditions. It was concluded that suitable thermoelastic and superelastic effects are achievable via appropriate selection of fixtured sintering conditions.

Keywords Compaction; Dimensional stability; Fixture; Hardness; Homogenous; Memory; Morphology; Near-net; Ni–Ti; Nitinol; Porosity; Powder metallurgy; Shape; Sintering; Workability.

Introduction

Shape memory behavior is the most attractive property of the NiTi phase. Because of considerable strength, ductility, toughness, hardness, resistance to corrosion, and biocompatibility, NiTi is now considered a successful biomaterial with applications in many industrial and biomedical devices such as robotic actuators, artificial hands, cardiovascular stents, double-cup hip prosthesis, laparoscopic surgical instruments, and dental archwires [1–7].

Thermomechanical work improves workability. High workability is required for production of wrought NiTi strips and wires with up to 8% recoverable pseudoelastic strain [8, 9]. Atmospheric gas [10], crucible contamination [11, 12], and compositional changes are critical to the workability; while compositional control makes TiNi production both complicated and costly [13].

Near-net-shape powder metallurgical (PM) processing is an attractive way to produce homogenous high purity NiTi intermetallic objects of specific shape [14–18]. NiTi surgical implants are good examples showing desirable osteo-integration capability [19] due to their unavoidable inherent porosity [20]. Low packing density and high dimensional change after sintering are, however, two undesirable drawbacks that should be improved [18]. The powder can for example be mechanically processed before compaction [21, 22]. Fixation of a pressed bimodal powder mixture during sintering is found to be helpful in this case [23, 24].

Received October 13, 2004; Accepted January 28, 2005
Address Correspondence to Sayed Khatiboleslam Sadrnezhaad, Department of Materials Science and Engineering, Sharif University of Technology, P.O. Box 11365-9466, Tehran, Iran; E-mail: sadrnezh@sharif.edu

Effects of sample compaction, sintering time, and sintering temperature on phase structure, internal porosity, dimensional stability, overall hardness, overall strength, and transformation temperatures of PM NiTi alloys are investigated through exact dimensional measurements, image analyses, hardness testing, X-ray diffraction (XRD), and differential scanning calorimetry (DSC) methods. The purpose of this study is to obtain the optimum conditions for production of near net-shape articles via powder metallurgy.

Experimental procedure

Nickel and titanium powders from Fluka, Switzerland and Merk, Gmbh of Germany with respective particle sizes of 3–5 and 21 μm and atomic ratio of 50/50 were blended together for around 1 hour in an eccentric shaker under argon. Cylindrical tablets, 15 mm in diameter and 1.9 to 2.3 mm in thickness, were made by bi-axial cold pressing of the mixture under different pressures. The compacts were then placed inside a carefully machined fixture made of DIN 1.4821 heat resistant steel and sintered at 950, 1000, and 1050°C for 7.2, 10.8, 14.4, and 18 kiloseconds under a continuous vacuum of better than 0.007 Pa. Schematics of the fixture are given in Fig. 1. Size, shape, and distribution of the Ti and Ni particles affect on porosity, density, and mechanical properties of the sintered sample. SEM micrographs of the powders used in this investigation are illustrated in Fig. 2. Uniform distribution combined with the differences in size and shapes of the metallic powders appropriates the formation of a condensed tablet suitable for subsequent sintering operation [18].

A pair of vernier calipers determined dimensional changes of the specimens during sintering. After sintering, the specimens were sectioned, ground, and polished using successive grades of SiC emery paper followed by 0.3 and 0.05 μm alumina powders. The apparent porosities of

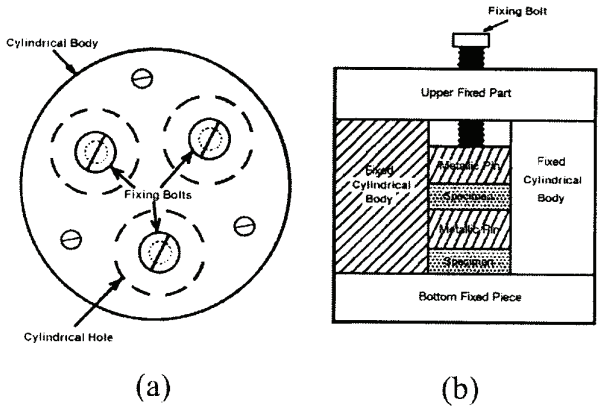

FIGURE 1.—Schematic representation of the fixture used for dimensional stability of Ni–Ti compacted sample during sintering: (a) top view and (b) side view.

the specimens were determined with an enhanced image analyzer from Bohler of England at a magnification of 400. Vickers hardness numbers were determined using a force of 49 N for macrohardness and 0.98 N for microhardness measurements.

Phase developments within the tablets due to sintering were inspected with a Philips X-ray diffractometer having a Co lamp of 1.7903 Å wavelength. Effects of compaction pressure, sintering time, and sintering temperature on morphology, microstructure, and transformation temperatures of the compacted/sintered samples were determined. Differential scanning calorimetry was used to measure these temperatures. Samples were thermally cycled within the range of 298 to 423 K at a heating/cooling rate of 0.083 K/s. Tensile tests were performed according to ASTM-E8 standard [25] for powder specimens.

RESULTS AND DISCUSSION

Figure 3 shows the effect of compaction pressure on the axial and radial dimensional changes of the samples after 2 hours of free and fixtured sintering at 1000°C. Each point is the average of six measurements. It can be seen that the use of the fixture diminishes both the rates of axial and radial changes of the specimens. The dimensional changes can be attributed to several processes such as phase transformation, porosity change, and interdiffusional effects.

The binary Ti–Ni diagram shown in Fig. 4 illustrates the thermodynamic conditions required for presence of B2, B19′, Ti_2Ni, and Ni_3Ti intermetallic phases at equilibrium [26]. $Ti_{90}Ni_{10}$ samples have, for example, shown small amounts of α-Ti together with Ti_2Ni embedded in β-Ti substrate [27]. TEM micrographs taken from quenched $Ti_{75}Ni_{25}$ samples have shown a stretched XRD peak together with very small β-Ti clusters scattered in an amorphous substrate [28]. In $Ti_{70}Ni_{30}$ samples, low cooling rate has resulted in small β-Ti particles scattered in Ti_2Ni substrate. High cooling rate has caused the formation of small β-Ti and Ti_2Ni phases embedded in an amorphous substrate.

Many authors have paid attention to effects of solidification rates on formation of Ti–Ni intermetallics in near equiatomic Ti–Ni binary alloy [26–28]. According to the equilibrium diagram, the equiatomic parent phase (B2) is stable at temperatures between 370 and 1600 K (Fig. 4a). This phase converts to B19′ at a temperature slightly above 370 K. Two invariant equilibria Ti_2Ni + B2 = B19′ (for $X_{Ni} \approx 0.49985$) and B2 = B19′ + Ni_3Ti (for $X_{Ni} \approx 0.49997$) can, however, result in formation of monoclinic B19′ martensite. Because of the very small temperature range associated with the two-phase region of B2 + B19′, the fast-cooling rate is not required for formation of equiatomic B19′ martensite in the Ti–Ni system [26].

Below 50% atom Ni, an increase in the nickel content can result in a small reduction in B2/B19′ transformation temperature. Tang [26] has calculated the temperature T_0 at which the Gibbs free energy of meta-stable B2 becomes equal to that of the stable B19′ phase [26]. Figure 4b demonstrates this temperature against the nickel content. It has been shown by Tang [26] that T_0 is nearly equal to the average of Ms and Af.

Sintered TiNi composed of B2 and/or B19′ is generally more porous than most other powder metallurgy alloys.

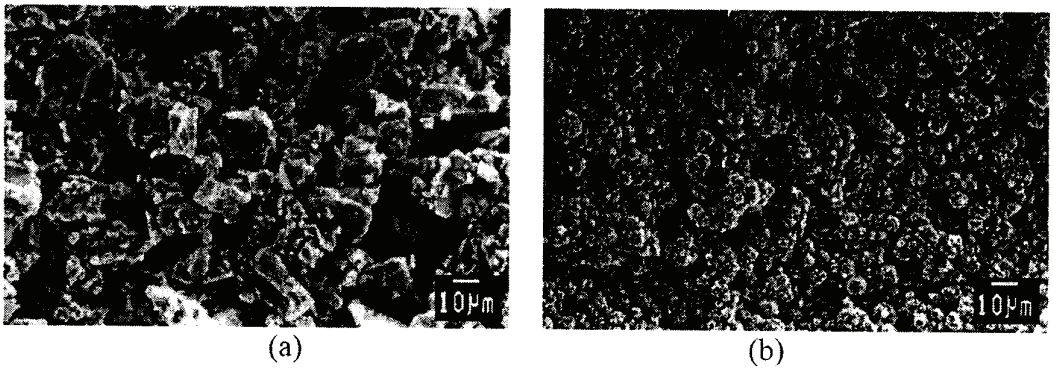

FIGURE 2.—Microstructure of raw materials used in this research: (a) Ti and (b) Ni.

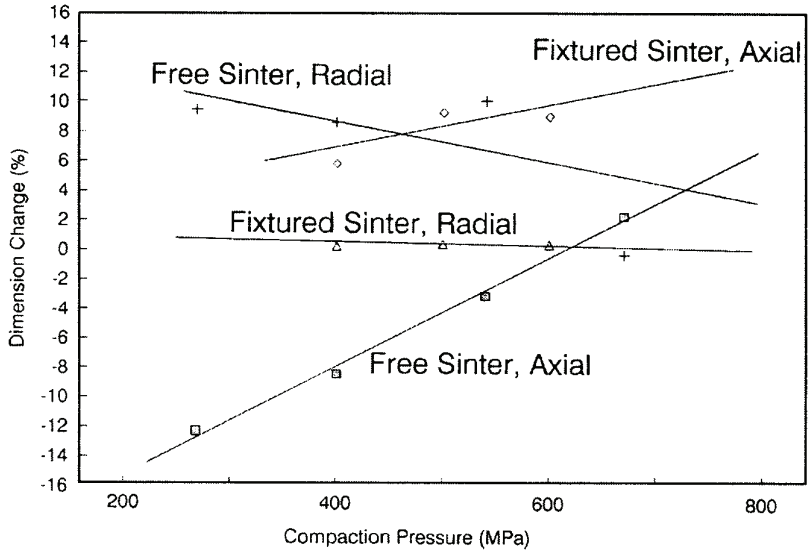

FIGURE 3.—Effect of compaction pressure and utilization of fixture on dimensional stability of the specimens sintered at 1000°C for 2 hours.

The reasons are as follows.

1. High porosity between green grains of Ti and Ni powders mixed together [29].
2. A larger intrinsic diffusion coefficient of nickel in titanium than that of titanium in nickel [30, 31]. This difference causes vacancy formation in the inter-diffusion zones of the sample [32].
3. Formation of new liquid-phase drops that accompany solidification shrinkage formation [32, 33].

Free liquid sintering is the main cause of dimensional change that occurs in both radial and axial directions of a TiNi specimen. During free liquid sintering, the specimen becomes semi-fluid and can move around almost freely. Formation of a new phase with different lattice parameters causes a volume change. This process causes dimensional changes in the specimen. Using a fixture can diminish this dimensional variation, but it cannot totally stop the size change.

Fixtured sintering can only reduce the dimensional changes of the specimens to some extent. A small change is therefore observed in dimensions of the samples with dimensional limitation imposed by a fixture. Imperfect seating of the fixed pins plus gradual wearing of the container with time could also result in a slight increase in dimensions of the samples observed in Fig. 3.

Fixtured sintering can diminish internal porosity by a particle collapsing action that is imposed by exertion of compaction pressure to the system. Figure 5 demonstrates the effect of fixture application on distribution and sizes of the pores in a TiNi-sintered mixture. Effect of compaction pressure and fixtured sintering on apparent amounts of porosity is demonstrated quantitatively in Fig. 6. Each point on the figure represents the average of five pore percentage measurements.

Figure 6 indicates the B2 formation reaction does not reach its completion with 2 hours sintering at 950°C. Maximum porosity percentage is, therefore, obtained at $t = 3$ hr. Releasing of the enthalpy of the phase formation reactions results in pore percentage enhancement at times lower than 3 hours. At $t = 3$ hr, the internal reactions reach their highest level, corresponding to the maximum pore percentage observation in the sample. Furtherance of the sintering treatment, at 950°C, results in decreasing porosity. This decrease is due to elimination of the thermodynamic tendency for more TiNi and other intermetallic phase formation.

Less than 2 hours of sintering at 1000°C is enough for completion of the Ni/Ti reaction. Extrapolation of the data plotted in Fig. 6 shows that this time may even be less, for fixtured sintering at 1050°C. Sintering at 1050°C results in a denser specimen compared to those sintered at lower temperatures. Free liquid movement at higher temperatures clearly shows a pronounced compaction effect. Less than 2 hours of sintering is sufficient, hence, for formation of the parent TiNi phase at both 1000 and 1050°C. Greater times can, however, help the formation of a denser specimen.

The XRD maps illustrated in Fig. 7 can explain the reasons behind the observed pore percentage quantities specified in Fig. 6. The B2 peak demonstrates a pure austenitic phase formation reaction at 1050°C (Fig. 7). The XRD spectra in Fig. 7 do not show any significant change in the angles and intensities of the peaks of the intermetallic phases during the sintering process at 1000°C. Figure 6 shows, however, that at 1000°C, the internal porosity of the samples decreases by further sintering of the compacted specimens. B2 phase growth under both high temperature and pressure can thus describe this effect.

Figure 6 shows the decrease in porosity of the samples by increasing the powder compaction pressure. This

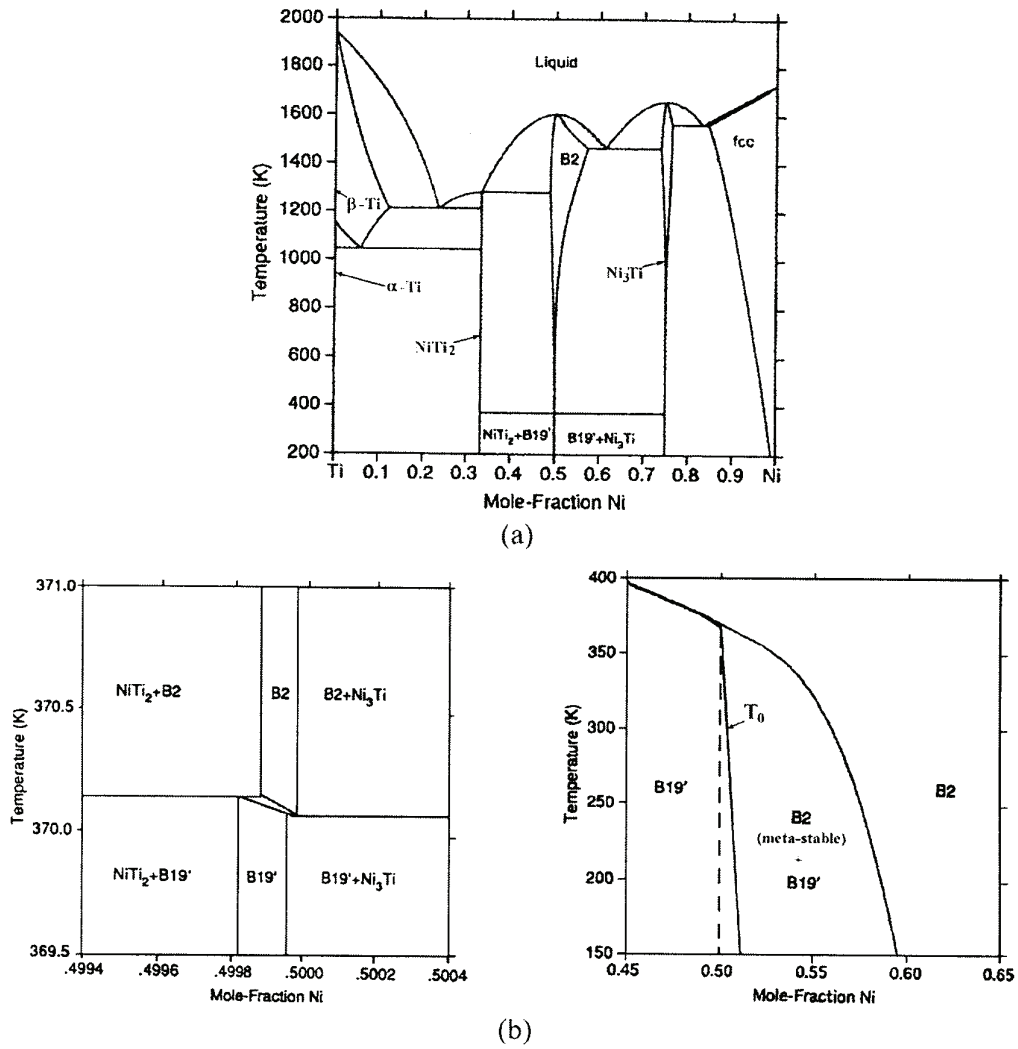

FIGURE 4.—Ni–Ti binary diagrams showing (a) equilibrium conditions for α-Ti, β-Ti, Ti_2Ni, B2, B19′, and $TiNi_3$phases and (b) stable and meta-stable B2 in equilibrium with Ti_2Ni, $TiNi_3$, and B19′ near ambient temperature, calculated by Tang [26].

phenomenon is metallographically illustrated in Fig. 8. Apparent pore changes are shown for specimens cold pressed at 500 MPa and fixture sintered at different times and temperature specified in this figure. The results are generalizable to the samples produced at other pressures.

Effect of utilization of a fixture on porosity of the samples is illustrated in Table 1. It is seen that fixturing reduces porosity percentages of the specimens at both 400 and 500 MPa compaction pressures. Similar to what is shown in Fig. 6, increasing the compaction pressure reduces the porosity percentages of the specimens.

Different parameters, such as the sintering time and temperature, the amount of the internal porosity, and the phase formation during sintering, influence the hardness of a sintered specimen. Experimental observations made on these effects are depicted in Fig. 9. It is seen from this figure that less than 3 hours of sintering at 950°C causes a decrease in the average hardness of the samples. This decrease can simply be attributed to the porosity increase in the same time range. More than 3 hours of sintering at 950°C causes, however, a hardness increase in all compacted samples. The internal porosity is, of course, decreased (Fig. 6) and the amount of hard precipitates may initially increase under these conditions (Fig. 7). The hard phases are, however, eliminated after 4 hours of sintering, based on the XRD graphs demonstrated in Fig. 7.

A simple comparison indicates that the average hardness of all specimens increases with compaction pressure (Fig. 9). At 1000 and 1050°C, longer sintering times show that the average hardness continuously decreases with

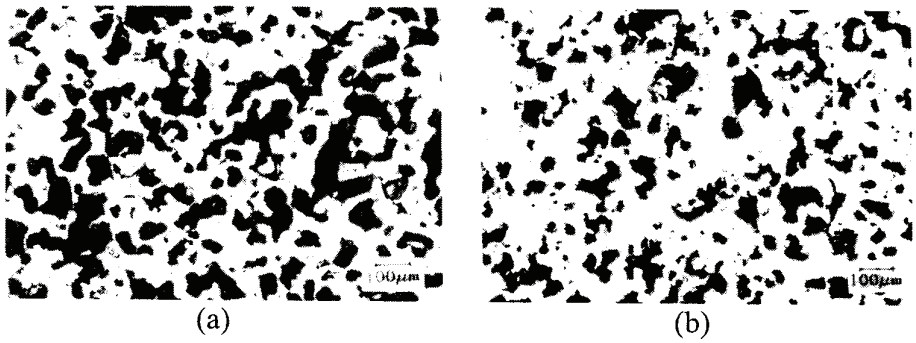

FIGURE 5.—Optical micrographs of the internal pores of the specimens produced at 400 MPa and sintered for 2 hours at 1000°C: (a) without fixture and (b) with a fixture.

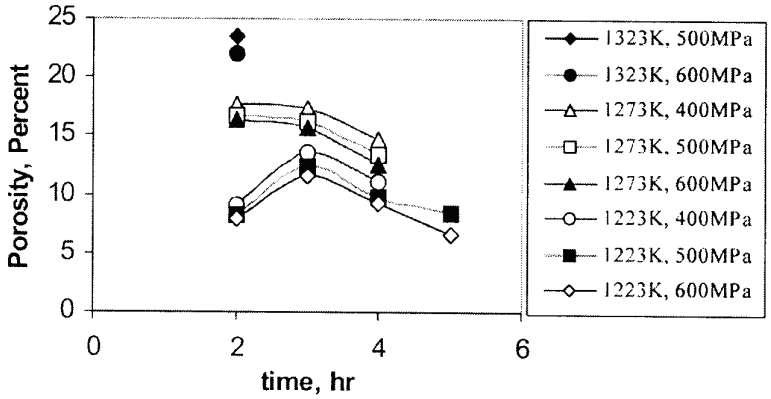

FIGURE 6.—Effect of compaction pressure and fixtured sintering conditions on apparent porosities of the specimens. Note that a shift of −5% is applied to the curves plotted for 1273 K and −10% to those plotted for 1223 K.

continued TiNi grain growth along with Ti_2Ni and $TiNi_3$ disappearance that would occur due to the continued transfer processes happening within the sample (Fig. 7). A higher sintering temperature would correspond to a softer sample.

Table 2 summarizes the phase transformation temperatures of the samples produced at different sintering temperatures. It is seen that all austenite/martensite transformation temperatures increase with increasing sintering temperature. Increasing the sintering temperature from 950°C to 1000°C or higher results in Ms movements towards a higher than ambient temperature (Table 2).

Increasing sintering temperature helps dissolution of the Ti_2Ni and $TiNi_3$ intermetallic phases usually precipitating during liquid-phase solidification. Formation of these undesirable precipitates can change the Ni/Ti ratio of the matrix to a greater number. This variation can increase both the phase transformation temperatures of the system and its hardness [34]. Any change that may alter the matrix composition of the system changes the transformation temperatures of the Ti–Ni memory alloy [35] and its equilibrium conditions (Fig. 4).

Previous studies have shown that transformation temperatures change when high temperature annealing of the TiNi results in formation of nonstoichiometric precipitates that can change the matrix composition of the specimens [34, 35]. Metallographic observations of the samples produced in this investigation showed that at 1050°C, the undesirable Ti_2Ni and $TiNi_3$ precipitates reduce to their minimum content. A prolonged sintering process seems to have a similar effect.

Depicted DSC diagrams of the alloy show extended thermal peaks. It is well known that these types of peaks are related to the porous nature of the specimens [36]. A local composition gradient existing within the porous specimens is a main cause for this phenomenon. Porous nitinol samples are nowadays known to be best suited for many medical applications [19]. With increasing alloy homogeneity, DSC peaks tend to become narrower and sharper [36]. This phenomenon is observed in our samples with increasing sintering temperature from 950 to 1050°C.

Micro-hardness results illustrated in Table 3 indicate that the Vickers hardness numbers of the parent phase decrease with both sintering time and temperature. Homogenization

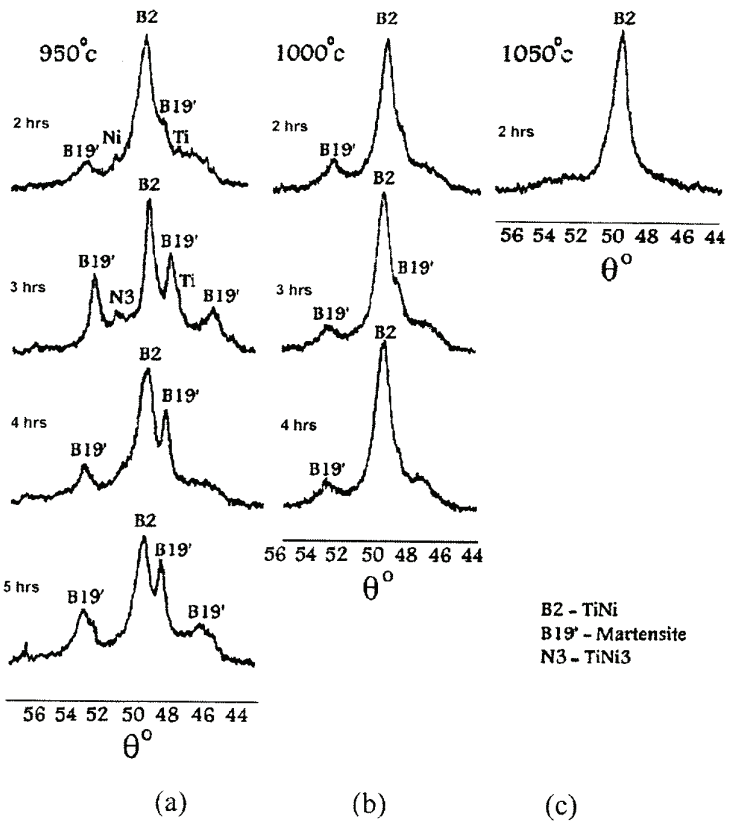

FIGURE 7.—Effect of sintering time and temperature on XRD peaks: (a) 950°C, (b) 1000°C, and (c) 1050°C.

of the sintered specimen and TiNi grain growth can best be understood to describe this interesting effect. Microhardness numbers given in Table 3 and phase equilibrium conditions specified in Fig. 4 both indicate that martensitic B19′ phase can be present at the ambient temperature. Metallographic pictures demonstrated in Fig. 10 confirm this conclusion. This phenomenon indicates that the sintered samples tend to a stress-induced martensitic transformation.

Effects of compaction pressure and sintering conditions on mechanical properties of the specimens are illustrated in Table 4. Mechanical property improvements are due to internal porosity reduction, which can result in remediation of the local stress concentrations during actual use of the sintered alloy specimens. These data indicate that the powder metallurgical route is an appropriate way to produce intricate medical objects that need sufficient yield and tensile strengths to hold two broken parts together. While fixtured sintering seems appropriate for production of low and medium force exerting specimens, it doesn't seem suitable for making those objects that require higher mechanical properties in application.

Utilization of a fixture for sintering of the objects benefits both geometrical stability and the mechanical properties of the specimens. Increasing the compaction pressure improves both mechanical strength and Young's modulus of the samples. Sintering time and temperature can both be utilized to optimize such properties as porosity, hardness, and microstructure of the specimen.

PRACTICAL APPLICATIONS

Powder metallurgy can overcome some of the traditional problems encountered in melting/casting of the Ti–Ni shape memory alloy. In-homogeneity, intermetallic precipitation, gas absorption, and carbon contamination are some of the well-known problems [10, 13]. High controlling power of powder metallurgy over chemical composition allows homogeneity improvement and inclusion elimination. Lower temperature and solid-state condition reduces the gas absorption and carbon contamination method.

Shape memory TiNi implants of specific geometry can be produced via liquid-phase sintering of compact blended powders. A limiting effect is the dimensional change. A fixtured process can diminish this problem. Experimental results show that increasing sintering temperature and time reduces pore percentage and improves mechanical properties of the specimen. Remaining porosity can be

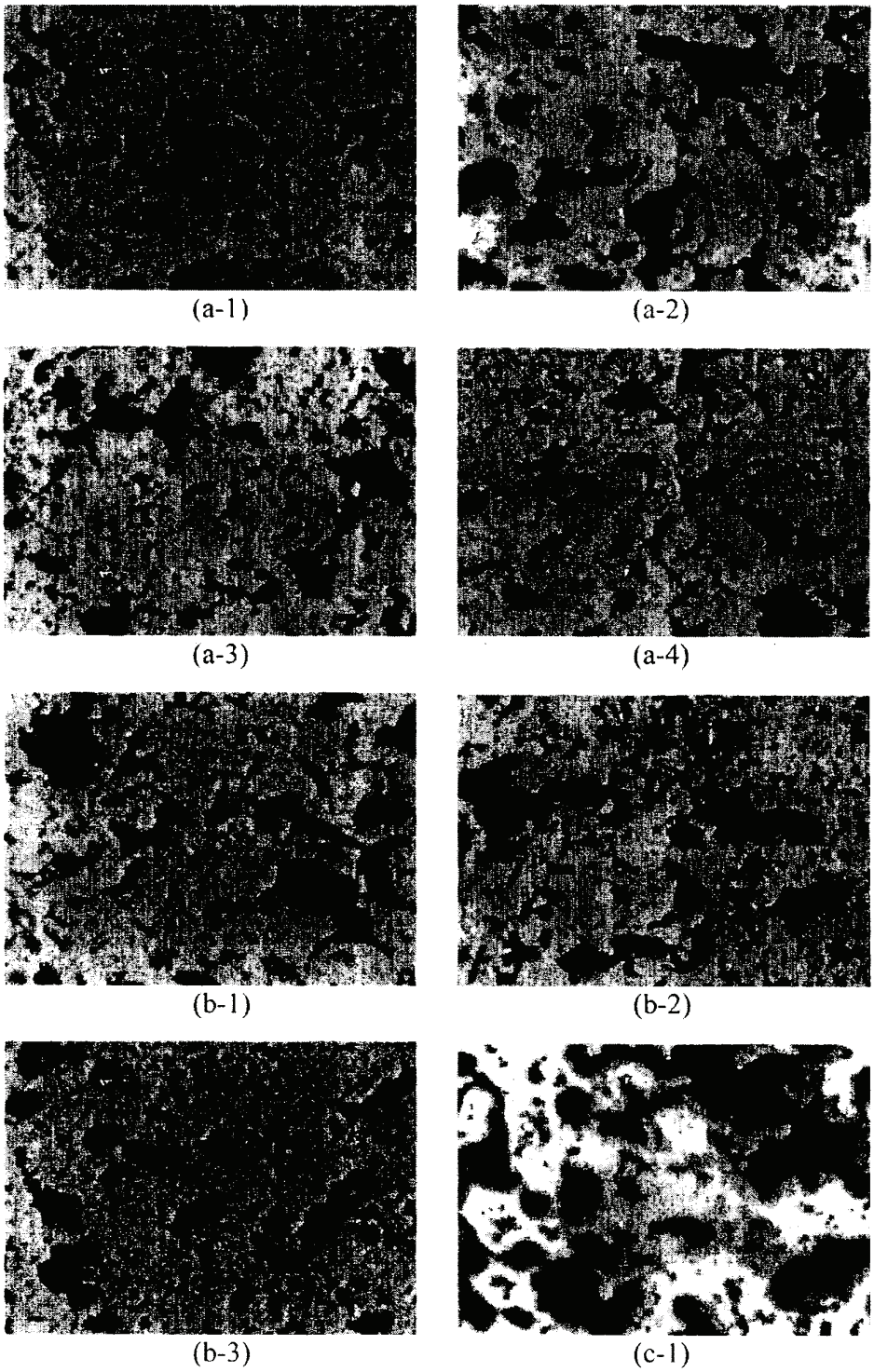

FIGURE 8.—Metallographic pictures taken at magnification of ×100 showing porosity of the specimens produced at 500 MPa and fixture sintered for (a-1) 2 hr at 950°C, (a-2) 3 hr at 950°C, (a-3) 4 hr at 950°C, (a-4) 5 hr at 950°C, (b-1) 2 hr at 1000°C, (b-2) 3 hr at 1000°C, (b-3) 4 hr at 1000°C, and (c-1) 2 hr at 1050°C.

TABLE 1.—Effect of fixturing and compaction pressure on porosity of the samples sintered for 2 hours at 1000°C.

Pressure (MPa)	Without fixture	With fixture
400	47.146	22.773
500	41.972	21.761

TABLE 2.—Transformation temperatures of the specimens fixture sintered for 2 hours at temperatures shown.

Temperature (°C)	Ms	Mf	As	Af
950	−10	−108	50	110
1000	61	−33	80	115
1050	70	−19	90	120

helpful to the osteo-integration capability of the sample [19]. Near-net-shape technology can benefit from conclusions of this research. Work is underway to develop the procedure further and to practically apply the results to production of biocompatible real components of biomaterial applications.

CONCLUSIONS

1. Powder metallurgy seems to be a suitable route for production of near-net-shape superelastic/shape memory parts useful in medical and engineering applications requiring clean, homogenous, inclusion-free, and geometrically stable TiNi alloys.
2. Using a fixture has interesting effects such as decreasing porosity, stabilizing dimensions, and strengthening of the sintered object.
3. Increasing the sintering temperature increases the production rate, decreases material loss, and favors the liquid-phase sintering of the desired TiNi phase.

TABLE 3.—Vickers micro-hardness results obtained from specimens compressed at 400 MPa and fixture sintered. Each point is the average of three measurements.

Temperature pressure (°C, MPa)	2 hr	3 hr	4 hr	5 hr
950, 400	297	265	241	–
1000, 400	260	220	199	–
950, 500	310	288	259	241
1000, 500	280	235	210	–
1050, 500	210	–	–	–

TABLE 4.—Tensile properties of specimens sintered at 1000°C for 4 hours.

Compaction pressure (Mpa)	Sintering condition	Y.S. Mpa	U.T.S. Mpa	E Gpa
180	Free	120	120	0.54
180	Fixtured	160	160	0.66
220	Fixtured	171	171	0.80

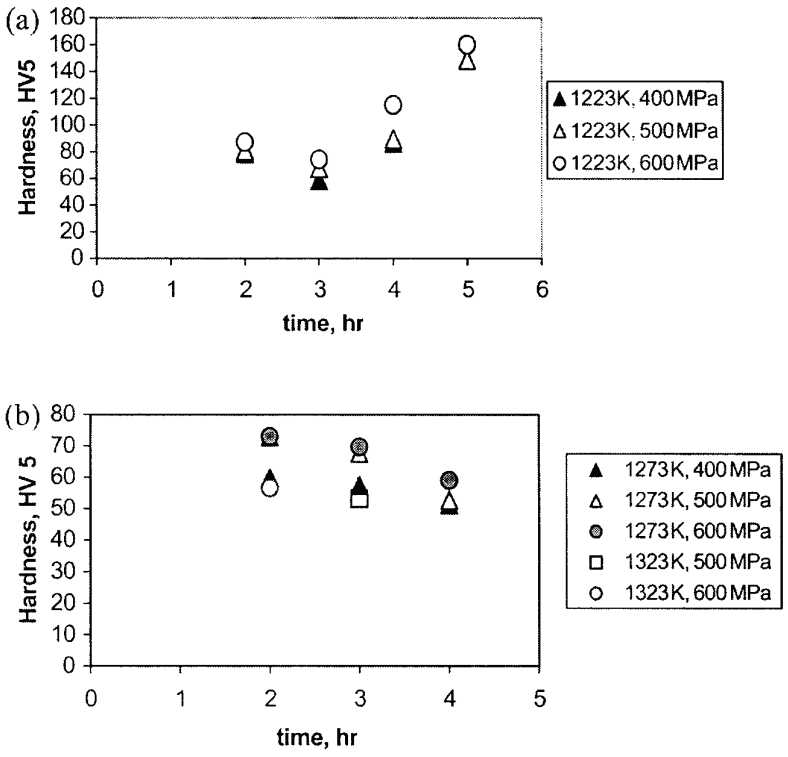

FIGURE 9.—Effect of compaction pressure and sintering time on average hardness of the specimens fixture sintered at: (a) 950°C and (b) 1000 and 1050°C.

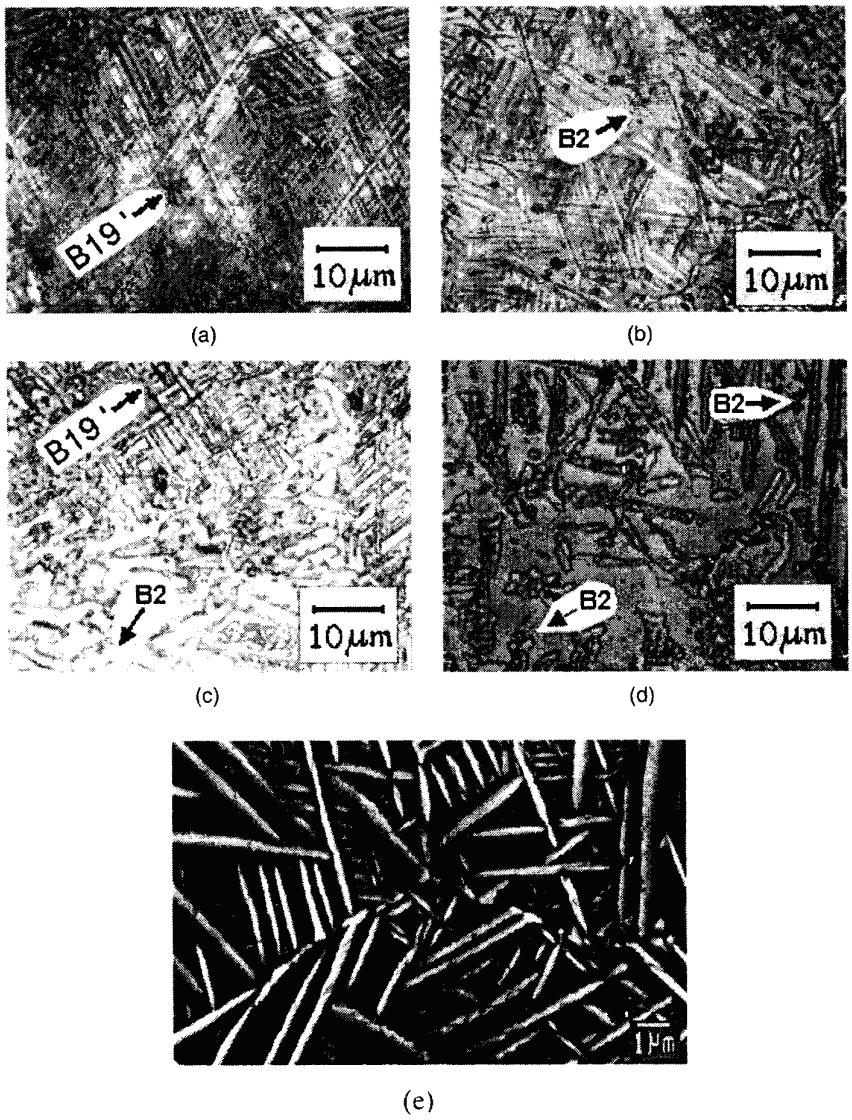

FIGURE 10.—Micrographs of specimens sintered for 2 hours at 1050°C: (a) austenitic matrix with partially produced martensite phase, (b) totally martensitic structure. (c) small amount of austenite 1 hr later formed in the same sample b, (d) large amount of austenite 20 hr later formed in the same sample b, and (e) SEM micrograph of the totally martensitic structure of b observed at ×7000 magnification.

4. Lengthy sintering results in a denser and less porous sample.
5. Increasing the compaction pressure decreases porosity; increases average hardness and enhances the strength of the specimens.
6. Empirical results show that both thermoelastic shape memory effect and superelastic stress-induced martensite effects are achievable via appropriate selection of the fixtured sintering conditions.

REFERENCES

1. Yinong, L. *Hysteretic Behavior of Thermoelastic Martensitic Transformation in Near-Equiatomic NiTi*; The Japan Institute of Metals: Japan, 2001; 1807–1811.
2. Brady, G.S. *Materials Handbook*, 14th Ed.; McGraw Hill Pub.: New York, 1997.
3. Duerig, T.; Pelton, A.; Stockel, D. An overview of Nitinol medical applications. Mater. Sci. Eng. **1999**, *273–275*, 149–160.

4. Li, Z.Q.; Sun, Q.P. Superelastic NiTi memory alloy micro-tube under tension-nucleation and propagation of martensite band. Key Engineering Materials **2000**, *177–180*, 461–466.
5. Thayer, T.A.; Bagby, M.D.; Moore, R.N.; DeAngelis, R.J. X-ray diffraction of Nitinol orthodontic arch wires. Am. J. Ortho. and Dentofacial Orthopedics **1995**, *June*, 604–611.
6. Rondelli, G.; Vicentitni, B. Localized corrosion behavior in simulated human body fluids of commercial Ni–Ti orthodontic wires. Biomaterials **1999**, *20*, 785–792.
7. Ryhanen, K.J.; Danilov, A.; Tuukkanen, J. Effect of nickel-titanium shape memory metal alloy on bone formation. Biomaterials **2001**, *22*, 2475–2480.
8. Yinong, L.; Favier, D. Stabilization of martensite due to shear deformation via variant reorientation in polycrystalline NiTi. Acta Mater. **2000**, *48*, 3488–4399.
9. Favier, D.; Yinong, L. Restoration by rapid overheating of thermally stabilized martensite of NiTi shape memory alloys. Journal of Alloys and Compounds **2000**, *297*, 114–121.
10. Rozner, G.; Heintzelman, E.F.; Buehler, W.J. Effect of addition of oxygen and hydrogen on microstructure and hardness of cast TiNi intermetallic compound. Trans. AIME **1965**, *58*, 415–418.
11. Schippereit, G.H.; Lang, R.M.; Kora, G.J. Status of the technology for casting titanium. AFS Trans. **1952**, *6* (5), 499–512.
12. Yi, H.C.; Moore, J.J. The combustion synthesis of Ni–Ti shape memory alloys. JOM **1989**, 31–37.
13. Raz, S.B.; Sadrnezhaad, S.K. Effects of VIM frequency on chemical composition, homogeneity and microstructure of NiTi shape memory alloy. Materials Science and Technology **2004**, *20* (5), 593–598.
14. Krone, L.; Schuller, E.; Bram, M.; Hamed, O.; Buchkremer, H.P.; Stover, D. Mechanical behavior of NiTi parts prepared by powder metallurgical methods. Materials Science and Engineering **2004**, *A378*, 185–190.
15. Li, B.Y.; Rong, L.J.; Li, Y.Y. Microstructure and superelasticity of porous Ni–Ti alloy. Science in China **1999**, *42* (1), 94–99.
16. Li, B.Y.; Rong, L.J.; Li, Y.Y.; Gjunter, V.E. Synthesis of porous Ni–Ti shape memory alloys by self-propagating high-temperature synthesis: reaction mechanism and anisotropy in pore structure. Acta Mater. **2000**, *48*, 3895–3904.
17. Li, B.Y.; Rong, L.J.; Li, Y.Y. Electric resistance phenomena in porous Ni–Ti shape memory alloys produced by SHS. Scripta Mater. **2001**, *44*, 823–827.
18. Green, S.M.; Grant, D.M.; Kelly, N.R. Powder metallurgical processing of Ni–Ti shape memory alloy. Powder Met. **1997**, *40* (1), 43–47.
19. Puleo, D.A.; Nanci, A. Understanding and controlling the bone-implant interface. Biomaterials **1999**, *20*, 2311–2321.
20. Li, B.Y.; Rong, L.J.; Li, Y.Y. Anisotropy of dimensional change and its corresponding improvement by addition of TiH_2 during elemental powder sintering of porous NiTi alloy. Materials Science and Engineering **1998**, *A255*, 70–74.
21. Maziarz, W.; Dutkiewicz, J.; Van Humbeeck, J.; Czeppe, T. Mechanically alloyed and hot pressed Ni-49.7 Ti alloy showing martensitic transformation. Materials Science and Engineering **2004**, *A375–378*, 844–848.
22. Sadrnezhaad, S.K.; Selahi, A.R. Effect of mechanical alloying and sintering on Ni–Ti powders. Materials and Manufacturing Processes **2004**, *19* (3), 475–486.
23. Uehara, S.; Sasano, H.; Kaiedo, Y.; Suzuki, T. Effect of hydrostatic pressure on the sintering behavior and density of blended elemental TiNi compacts. Powder Met. Inter. **1985**, *17* (5), 229–232.
24. Morris, D.G.; Morris, M.A. NiTi Intermetallic by mixing, milling and interdiffusing elemental components. Mater. Sci. Eng. A **1989**, *110*, 139–149.
25. Annual Book of ASTM Standard–Metals Test Methods and Analytical Procedures, 1990, *03.01*.
26. Tang, W. Thermodynamic study of the low-temperature phase, B19′ and martensitic transformation in near equiatomic Ti–Ni shape memory alloys. Metal. Mater. Trans. A **1997**, *28A*, 537–544.
27. Sluiter, M.; Turchi, F.J. Pinski; Stock, G.M. A first principles study of phase stability in Ni–Al and Ni–Ti alloys. Mater. Sci. Eng. A **1992**, *152*, 1–8.
28. Nagarjan, R. Microstructural development in rapidly solidified Ti–Ni alloys. Mater. Sci. Eng. A **1994**, *179/180*, 198–204.
29. Hey, J.C.; Jardine, A.P. Shape memory TiNi synthesis from elemental powders. Mater. Sci. Eng. **1994**, *A188*, 291–300.
30. Bastin, G.F.; Rieck, G.D. Diffusion in the titanium-nickel system: Part 1. Metal. Trans. A **1974**, *5*, 1817–1826.
31. Bastin, G.F.; Rieck, G.D. Diffusion in the titanium-nickel system: Part 2. Metal. Trans. A **1974**, *5*, 1827–1831.
32. Shewmon, P.G. *Diffusion in Solids*; McGraw Hill Pub.: New York, 1996.
33. Igharo, M.; Wood, J.V. Compaction and sintering phenomena in titanium-nickel shape memory alloys. Powder Met. **1985**, *28* (3), 131–139.
34. Sadrnezhaad, K.; Mashhadi, F.; Sharghi, R. Heat treatment of Ni–Ti alloy for improvement of shape memory effect. Materials and Manufacturing Processes **1997**, *12* (1), 107–115.
35. Zarandi, F.M.H.; Sadrnezhaad, K. Thermomechanical study in combustion synthesized Ti–Ni shape memory alloy. Materials and Manufacturing Processes **1997**, *12* (6), 1093–1105.
36. Li, B.Y.; Rong, L.J.; Luo, X.H.; Li, Y.Y. Transformation behavior of sintered porous NiTi alloys. Metal. Mater. Trans. A **1999**, *30A*, 2735–2756.